



Various mechanisms to induce present-day shallow flat subduction and implications for the younger Earth: a numerical parameter study

Jeroen van Hunen^{a,*}, Arie P. van den Berg^b, Nico J. Vlaar^b

^a *Institut für Geophysik, ETH Hönggerberg (HPP), CH-8093, Zürich, Switzerland*

^b *Department of Theoretical Geophysics, Institute of Earth Sciences, Utrecht University, Utrecht 3508 TA, The Netherlands*

Received 31 August 2002; accepted 31 July 2003

Abstract

Shallow flat subduction is a relatively common feature at present-day subduction zones. Several mechanisms to explain this feature have been proposed, and can be subdivided into three groups: overthrusting of the subducting plate, subduction of a plume-generated oceanic plateau, and slab suction forces. We developed a numerical model to investigate these mechanisms and tested it through a comparison of the model results with the observations of the Peru flat slab where all three mechanisms seem to be contributing. The ratio of contributions of overthrusting continent to plateau subduction is in the range of 1:1 to 1:2, and the role of plate suction forces is likely to be significant. By applying the overthrusting continent and plateau subduction mechanisms separately, we were able to determine the most important model parameters for each of the mechanisms. Overthrusting easily results in flat subduction, and the flat slab length is primarily a function of slab age, overriding plate motion and mantle viscosity. An oceanic plateau is much less likely to cause flat subduction, and favorable conditions for flat subduction include a young slab age, long-lived plateau buoyancy after subduction, a strong mantle, and addition of slab suction forces that are large enough to further reduce the subduction dip angle, once the plateau initiates this flattening. Furthermore, we found that even though today flat subduction can be explained with the dominant model parameters within a reasonable range, for a slightly hotter, younger Earth, these flat subduction conditions are much less favorable, and so this style of subduction was probably not present in the past. This contradicts earlier predictions that flat subduction was a more wide-spread phenomenon in the early stages of plate tectonics in a younger earth.

© 2004 Elsevier B.V. All rights reserved.

Keywords: Shallow flat subduction; Plume-generated oceanic plateau

1. Introduction

The phenomenon of shallow flat subduction occurs at several present-day convergence zones. The best-known example is the horizontally subducting

slab below South Peru. At this location, the Nazca plate subducts with a normal dip angle of about 14° (Jarrard, 1986) to a depth of about 100 km, from where it bends back to the horizontal and moves with zero dip angle as far as 700 km inland (Sacks, 1983; Gutscher et al., 2000). Other areas include Central Chile, Central Mexico, Cascades, and the Nankai Trough (Jarrard, 1986; Gutscher et al., 2000). From

* Corresponding author. Tel.: +41-1-6336623.

E-mail address: hunen@erdw.ethz.ch (J. van Hunen).

geological observations it has been suggested that a very large flat slab was present below the Western United States around 65 Ma ago (Cross and Pilger, 1978; Bird, 1988; Spencer, 1996). Most other subduction zones show subduction with a much steeper dip angle (Jarrard, 1986). Since slab pull, the negative buoyancy of the dense subducting slab, is most likely the dominant driving force of plate motion (Wortel et al., 1991), these steep slabs are more in agreement with what we would expect from buoyancy considerations alone. Shallow flat subduction does not fit in this simple picture, and additional mechanisms, mostly based on correlation and observations (Jarrard, 1986), are proposed to provide a better explanation.

We can group these mechanisms into three categories. The first category assumes that the buoyancy of the subducting plate helps to keep the slab at shallow depth and more or less horizontal (Cross and Pilger, 1978). Young slab age reduces its average density, and therefore also its negative buoyancy. Most shallow flat slabs are indeed not older than 40 to 50 Ma (Vlaar and Wortel, 1976; Jarrard, 1986). Oceanic plateaus form another cause for low slab density. Their thicker-than-average crust and underlying harzburgite layer (which are both less dense than normal mantle material) significantly decrease the average density of the plate. Correlation between several subducting plateaus and flat slab areas suggest that indeed such plateaus could significantly reduce the dip angle. These plateaus are most likely the result of a hot mantle plume below the lithosphere. The plume locally increases the average mantle temperature, and therefore also the amount of partial melt and melt residue that is created. In this way, the interaction of a mantle plume and a mid ocean ridge leads to a thicker oceanic crust and harzburgite layer (Saunders et al., 1996), but the large heat source of plume heads can probably also produce an oceanic plateau on older, already existing oceanic lithosphere.

A second explanation uses the trenchward motion of the overlying plate as a means to explain flat subduction. Correlation between continental motion in a hot spot reference frame and the dip angle of neighboring slabs again suggest such causal relation (Cross and Pilger, 1978). Vlaar (1983) proposed a ‘lithospheric doubling’ scenario, in which a conti-

nent actively moves in the direction of a trench, and overthrusts relatively young oceanic lithosphere. The underplated material does not have sufficient negative buoyancy to sink quickly deeper into the mantle, and this situation may lead to flat subduction.

Finally, non-hydrostatic pressure forces, or ‘slab suction forces’ are proposed as a possible explanation (Stevenson and Turner, 1977; Tovish et al., 1978). Although in principle these forces apply at any trench, the effect would be largest in already shallowly dipping slabs, which could flatten those slabs completely and could explain the absence of dip angles between 10 and 20° (Tovish et al., 1978).

Flat subduction has also been suggested as the dominant subduction style in a younger hotter Earth (Vlaar, 1986; Abbott et al., 1994). In the past, the mantle temperature was higher than today. Since the 1980’s, there has been an ongoing debate about the actual amount of cooling since the Archean (England and Bickle, 1984; Bickle, 1986; Vlaar, 1986; Herzberg, 1992; de Wit, 1998; Hamilton, 1998), and proposed temperature drops range from 50 to 350 K. This higher mantle temperature may have important consequences for the subduction dynamics in the past. On the one hand, it leads to more partial melting of mantle material near the mid-ocean ridges and thus thicker crust and harzburgite layers, similar to the present-day oceanic plateaus. On the other hand, mantle viscosity drops with increasing temperature. These phenomena have raised questions about the viability of plate tectonics in the past (Vlaar, 1986; Vlaar and van den Berg, 1991; Davies, 1992). Here, we focus on the effect of an increased mantle temperature on the subduction dip angle of underthrust lithosphere.

Here, we first investigate the mechanisms and viability of flat subduction in a series of numerical modeling experiments. In the next section, the numerical model setup is described. In Section 3, results of earlier studies are combined with new results to better identify the characteristics of each of the proposed flat-subduction mechanisms. We compare the modeling results to observations of the Peru flat slab area, and use this model to further investigate the effects of the proposed mechanisms separately. In Section 4, we apply the model to a younger, hotter Earth to examine the viability of shallow flat subduction in the past.

2. Model description and numerical methods

2.1. The set of governing equations

To solve for the dynamics of the moving lithosphere, slab, and surrounding mantle, conservation laws for mass and momentum are used:

$$\partial_j u_j = 0 \quad (1)$$

$$\partial_j(\eta \dot{\epsilon}_{ij}) - \partial_i \Delta P = \Delta \rho g_i \quad (2)$$

where $\Delta P = p - \rho_0 g z$ is the dynamic pressure, and the effective density variations $\Delta \rho$ and viscosity η are elaborated below. All symbols are described in Table 1. The flow field is dependent on temperature through several temperature-dependent physical parameters and mechanisms, such as viscosity, buoyancy, phase-transitions in mantle and crust, and shear heating. Temperature is solved using conservation of energy:

$$\rho_0 c_p \left(\frac{\partial T}{\partial t} + u_j \partial_j T \right) - \alpha T \frac{dp}{dt} - \sum_k \frac{\rho_0 T \gamma_k \delta \rho_k}{\rho_0^2} \frac{d\Gamma_k}{dt} - \partial_j(k \partial_j T) = \tau_{ij} \partial_j u_i + \rho_0 H \quad (3)$$

Furthermore, with a purely advective transport equation, we track a material field throughout the model domain to enable the definition of material-dependent properties (e.g. viscosity and buoyancy):

$$\frac{\partial C}{\partial t} + u_j \partial_j C = 0 \quad (4)$$

which is solved with a tracer particle method. This set of equations is non-dimensionalised with the following scaling scheme:

$$\bar{x} = \bar{x}' h, \quad t = t' \frac{h^2}{\kappa}, \quad \bar{u} = \bar{u}' \frac{\kappa}{h}, \quad T = T_s + T' \Delta T$$

2.2. Buoyancy and viscosity definitions

In this model, the mantle dynamics are predominantly driven by internal buoyancy forces and external imposed plate velocities. The buoyancy is determined by internal density variation

$$\Delta \rho(T, C, \Gamma_k) = \rho_0 \left[-\alpha(T - T_s) + \frac{\Delta \rho_c}{\rho_0} + \sum_k \frac{\delta \rho_k}{\rho_0} \Gamma_k \right] \quad (5)$$

which describes three different origins: thermal, compositional and due to phase transitions, respectively. The incorporated phase transitions are described in Section 2.3.

A key physical parameter in the dynamics of mantle and lithosphere is the rheology. Olivine controls to a large extent the strength of mantle material, while crustal strength is on average much lower, and best described by the strength of basalt, its coarse-grain size equivalent gabbro, or, at depth, eclogite (see below). Dominant creep flow mechanisms are diffusion creep, dislocation creep, and possibly a stress-limiting deformation mechanism that controls the maximum strength of cold material (Karato et al., 2001). We applied a composite rheology formulation (van den Berg et al., 1993) to describe the combined effects of these mechanisms. A general Arrhenius expression:

$$\eta = A^{-1/n} \dot{\epsilon}^{(1-n)/n} \exp \left[\frac{E^* + pV^*}{nRT} \right] \quad (6)$$

describes the diffusion or dislocation creep components for mantle or crustal materials. Parameters are taken from (Karato and Wu, 1993) and the prefactor A and activation volume V^* are modified somewhat to meet the constraints from post-glacial rebound models. These models suggest an upper mantle viscosity ranging between 2.6 and 4.6×10^{20} Pa s and a lower mantle viscosity between 4×10^{21} and 3×10^{22} Pa s (Lambeck and Johnston, 1998; Lambeck et al., 1998) (see Fig. 1). True polar wander data in combination with geoid inversions predict an upper mantle viscosity somewhat higher than 10^{20} Pa s (Vermeersen et al., 1998). Applied rheological parameters for the different model setups are given in Table 2. Some models contain a subduction mantle wedge that is weakened with respect to the rest of the mantle, to account for the weakening effect of hydrous minerals in the wedge, and its details are described below. All oceanic crust is underlain by a depleted harzburgite layer (see Section 2.4), which is assigned the same rheology as normal (i.e. undepleted) mantle material.

Although not as extensively studied as olivine, laboratory deformation studies are also performed for oceanic crust by (e.g.) Shelton and Tullis (1981), Caristan (1982), and, under completely dry conditions, by Mackwell et al. (1998). Uncertainties, however, are in general much higher for crustal material, because of widely varying grain size and hydration.

Table 1
Notations

Symbol	Meaning	Value used	Dimension
A	pre-exponential flow law parameter	–	$\text{Pa}^{-n} \text{s}^{-1}$
C	composition parameter	–	–
c_p	specific heat	1250	$\text{J kg}^{-1} \text{K}^{-1}$
E^*	rheological activation energy	–	J mol^{-1}
H	radiogenic heat production	–	W m^{-3}
h	depth of the model domain	2000	km
k	thermal conductivity	4.27	$\text{W m}^{-1} \text{K}^{-1}$
n	viscosity stress exponent	–	–
n_y	yield stress exponent	5	–
p	pressure	–	Pa
R	gas constant	8.3143	$\text{J K}^{-1} \text{m}^{-3}$
T	absolute temperature	–	K
T_0	non-dimensional surface temperature $T_s/\Delta T$	0.119	–
T_s	dimensional surface temperature	273	K
T_{tr}	transition temperature for the eclogitisation reaction	–	$^{\circ}\text{C}$
t	time	–	s
t_{tr}	transition time for the eclogitisation reaction	10	Ma
\vec{u}	velocity $\vec{u} = (v, w)^T$	–	m s^{-1}
V^*	activation volume	–	$\text{m}^3 \text{mol}^{-1}$
v_{ov}	overriding velocity of the overlying plate	–	cm y^{-1}
v_{subd}	subduction (or convergence) velocity	–	cm y^{-1}
α	thermal expansion coefficient	3×10^{-5}	K^{-1}
Γ_k	phase function for the k th mantle phase transition	–	–
γ_k	Clapeyron slope of the k th phase transition		
	400 km phase transition	3	MPa K^{-1}
	670 km phase transition	–2.5	MPa K^{-1}
ΔP	hydrodynamic pressure	–	–
ΔT	vertical temperature contrast across model domain	2300	K
$\Delta \rho$	total density variation with respect to ρ_0	–	kg m^{-3}
$\Delta \rho_c$	compositional density relative to mantle material		
	basalt	–400	kg m^{-3}
	harzburgite	–77	kg m^{-3}
$\delta \rho_k$	density difference across the k th phase transition		
	400 km phase transition	273	kg m^{-3}
	670 km phase transition	342	kg m^{-3}
$\dot{\epsilon}_{ij}$	$\dot{\epsilon}_{ij} = \partial_j u_i + \partial_i u_j =$ strain rate tensor	–	s^{-1}
$\dot{\epsilon}$	2nd invariant of the strain rate	–	s^{-1}
$\dot{\epsilon}_y$	reference strain rate in yield stress determination	10^{-15}	s^{-1}
η	viscosity	–	Pa s
η_0	reference viscosity	10^{21}	Pa s
η_y	yield viscosity	–	Pa s
$\bar{\eta}_{\text{UM}}$	average upper mantle viscosity	–	Pa s
κ	thermal diffusivity	10^{-6}	$\text{m}^2 \text{s}^{-1}$
ρ_0	reference mantle density	3416	kg m^{-3}
τ_y	yield stress	–	Pa
σ_{ij}	total stress tensor $\sigma_{ij} = -p\delta_{ij} + \tau_{ij}$	–	Pa
τ_{ij}	deviatoric stress tensor	–	Pa
τ	2nd invariant of the stress tensor τ_{ij}	–	Pa
τ_y	yield stress for strain rate $\dot{\epsilon}_y$	–	Pa

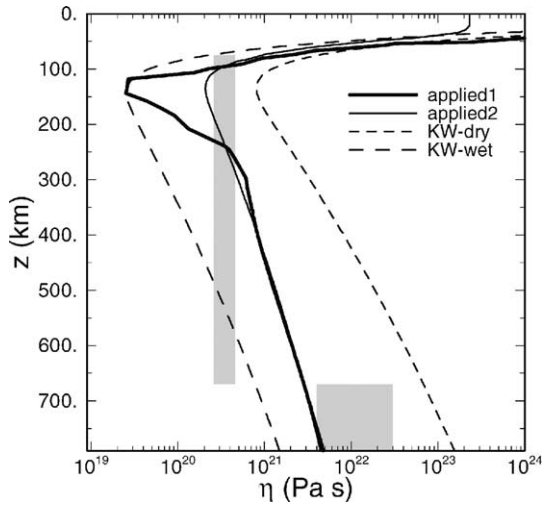


Fig. 1. Compilation of vertical viscosity profiles through a 40-Ma old oceanic lithosphere in a mantle with a 1300 °C-potential temperature. The thick solid line is a typical profile example from model calculations (free $\dot{\epsilon}$). Using the same rheological parameters, the thin solid line gives a profile in case of a constant strain rate $\dot{\epsilon} = 10^{-15} \text{ s}^{-1}$ (fixed $\dot{\epsilon}$). Dashed lines represent the wet (KW-wet) and dry (KW-dry) profiles for rheological parameters from (Karato and Wu, 1993) (using $\mu = 80 \text{ GPa}$, $b = 0.5 \text{ nm}$, $d = 1 \text{ mm}$ and $m = 2.5$) for $\dot{\epsilon} = 10^{-15} \text{ s}^{-1}$. The gray areas give the effective viscosity, as proposed by Lambeck et al. (1998) from post-glacial rebound results.

We adopted the dislocation flow law from Shelton and Tullis (1981), but changed the prefactor to lower the crustal strength to meet the requirement that the crust should be weak enough to decouple the two approaching lithospheres at a subduction zone (van

Hunen et al., 2000). Basalt transforms to eclogite during subduction (see below), of which the rheology is even less well known than for basalt: Ji and Zhao (1994) report strong eclogite, while Stöckhert and Renner (1998) find eclogite to be weak in comparison to basalt. We decided to assign the same strength to basalt and eclogite.

Slabs would be much too strong to deform in the mantle, if only (depth-dependent) diffusion and dislocation creep mechanisms are applied (Cížková et al., 2002). We have included here a general stress-limiting deformation mechanism to account for brittle or semi-brittle deformation (Kohlstedt et al., 1995; Bos and Spiers, 2002), or low-temperature plasticity (or Peierl’s stress mechanism, see Kameyama et al., 1999; Karato et al., 2001). To do so, we define a yield viscosity η_y as:

$$\eta_y = \tau_y \dot{\epsilon}_y^{-1/n_y} \dot{\epsilon}^{1/n_y - 1} \quad (7)$$

in which the ‘brittleness’ of this deformation mechanism is described by n_y , which was chosen to be 5 in this study. Other parameters and their applied values are given in Table 1.

2.3. Major phase transitions in mantle and crust

The major mantle phase transitions around 400 and 670 km depth are implemented (van Hunen et al., 2001), including the latent heat effects, which can both favor and resist vertical motion of slabs. The relatively young age of the slabs in this study does not

Table 2

Rheology parameters for the deformation mechanisms of crust and mantle material for different average upper mantle viscosity values $\bar{\eta}_{UM}$

Material	Mechanism	A (Pa ⁻ⁿ s ⁻¹)	n	E* (J mol ⁻¹)	V* (cm ³ mol ⁻¹)
Crust	Dislocation creep		3.4	260 × 10 ³	10
	$\bar{\eta}_{UM} < 10^{21} \text{ Pa s}$	8.8×10^{-18}			
	$\bar{\eta}_{UM} = 10^{21} \text{ Pa s}$	8.8×10^{-19}			
Mantle	Diffusion creep		1.0	300 × 10 ³	4.5
	$\bar{\eta}_{UM} = 2 \times 10^{20} \text{ Pa s}$	2.42×10^{-10}			
	$\bar{\eta}_{UM} = 3.5 \times 10^{20} \text{ Pa s}$	1.21×10^{-10}			
	$\bar{\eta}_{UM} = 6.5 \times 10^{20} \text{ Pa s}$	6.07×10^{-11}			
Mantle	Dislocation creep		3.5	540 × 10 ³	14
	$\bar{\eta}_{UM} = 2 \times 10^{20} \text{ Pa s}$	3.05×10^{-15}			
	$\bar{\eta}_{UM} = 3.5 \times 10^{20} \text{ Pa s}$	1.53×10^{-15}			
	$\bar{\eta}_{UM} = 6.5 \times 10^{20} \text{ Pa s}$	7.6×10^{-16}			

Crustal diffusion creep is not applied.

require olivine-metastability to be taken into account (Schmeling et al., 1999).

The ‘buoyant-slab’ theory which explains the occurrence of flat slabs by the buoyancy of the subducting plate requires that this slab remains buoyant for several millions of years after subduction, and until a depth of at least 100 km. The main contribution to this buoyancy comes from the basaltic crust. It is, however, known that under equilibrium conditions, basalt transforms into eclogite at a depth of about 50 km. Basalt is approximately 400 kg m^{-3} less dense than mantle material, whereas eclogite is about 200 kg m^{-3} more dense than mantle material. This implies that most or all of the compositional buoyancy of the slab will be lost after this crustal phase transition. Geological observations, however, suggest that basalt can persist in a metastable phase in the eclogite stability field. Although this metastability is not yet well quantified, metastable basalt may exist for temperatures below $400\text{--}800^\circ\text{C}$, under relatively dry conditions, and without too much deformation (Ahrens and Schubert, 1975; Rubie, 1990; Hacker, 1996; Austrheim, 1998).

Such phase change kinetics are generally described by a nucleation and growth theory (Riedel and Karato, 1996). A simplified parameterization was proposed by (Giunchi and Ricard, 1999), and we adopted their method, and applied it to describe the eclogitisation of the subducting oceanic crust (van Hunen et al., 2002b). A ‘transition temperature’ T_{tr} was defined to conveniently express the reaction rate, and displays the temperature at which half of the reaction takes place in a rather arbitrarily chosen reaction time or ‘transition time’ $t_{\text{tr}} = 10 \text{ Ma}$. This is a significant time span in subduction zone processes, and T_{tr} can therefore also be seen as the maximum temperature that basalt is able to survive. For higher temperatures $T > T_{\text{tr}}$, the reaction is much faster (i.e. the reaction time $< t_{\text{tr}}$), while for lower temperatures, it is slower.

2.4. Model geometry and boundary conditions

A Cartesian two-dimensional (2-D) model domain of 5200 km wide and 2000 km deep is used to model the subduction process (Fig. 2). A fully decoupling 100 km deep fault with a static arc-shaped geometry separates the oceanic lithosphere on the left from the overriding continent on the right. The overthrusting motion of the continent is prescribed in a reference

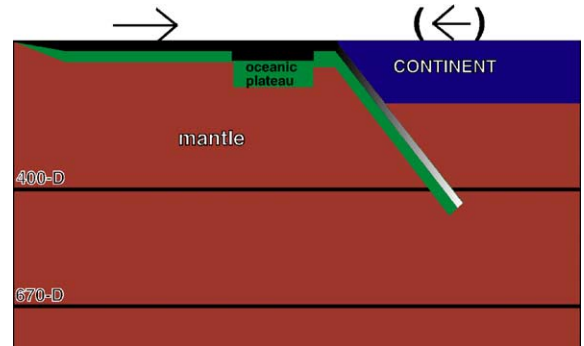


Fig. 2. Sketch of the numerical model geometry. A 100-km deep free-slip fault decouples the oceanic lithosphere from the continental one. The oceanic plate is compositionally subdivided into a crust-harzburgite-lherzolite layered system. If applied, an oceanic plateau with thicker crust and harzburgite layers is part of the subducting plate and is about to enter the subduction zone at model time $t = 0$. The major mantle phase transitions at 400 and 670 km depth are incorporated, as well as a (kinetically delayed) basalt-to-eclogite transition in the oceanic crust.

frame attached to this continent (van Hunen et al., 2000). Modeling of an essentially three-dimensional oceanic plateau in a 2-D model requires imposed subducting plate velocities at the surface to avoid the overestimation of the plateau effect on the convergence rate (van Hunen et al., 2002b): a free-slip condition would be inappropriate, because the subduction would stop as soon as the plateau enters the subduction zone, while in the full, 3-D situation, the convergence is determined by the (negative) buoyancy of the much larger remainder (outside the buoyant plateau) of the subducting plate. The left hand boundary becomes an ‘inflow’ boundary, in case of a modeled overthrusting continent, which is defined by $v_x = -v_{\text{ov}}$ and $\sigma_{xz} = 0$ boundary conditions on the inflow boundary. On the right hand boundary, a ‘horizontal, developed outflow’ boundary condition is imposed: $\sigma_{xx} = -p$ and $v_z = 0$. The bottom boundary is impermeable and has the same prescribed horizontal flow as the left hand boundary. Temperature $T = 0^\circ\text{C}$ at the top, and follows a mantle adiabat for a given potential temperature at the bottom and left hand boundary. The right hand boundary has ‘reflecting’ thermal boundary conditions: $\partial T / \partial x = 0$. The initial temperature distribution is adiabatic with a given potential temperature T_{pot} , on which a cool top layer is superimposed: a cooling halfspace solution for the oceanic lithosphere,

and for the continental lithosphere a steady state temperature distribution with crustal radiogenic heat production according to (Chapman, 1986), corresponding to a 60 mW m^{-2} surface heat flow. For normal oceanic lithosphere, the crust is 7 km thick, and is underlain by an 18-km thick depleted harzburgite layer with a compositional density difference of -77 kg m^{-3} with respect to undepleted mantle material. In an oceanic plateau, the crust is thickened to 18 km, and the underlying harzburgite layer is thickened proportionally. The lateral extent of a plateau is fixed to 400 km.

In this study, we report two sets of experiments: set I is to examine the significance of several physical quantities in the development of shallow flat slabs in present-day subduction zones, and determine the relative importance of the proposed flattening mechanisms. Set II examines the viability of flat subduction in a hotter, younger Earth. Set I is performed in two steps. The initial step is done once, in which a subducting slab is formed. We start with an oceanic and continental lithosphere neighboring each other, and force the oceanic plate to subduct below the continent until the tip has just reached the 400 km phase transition. We used the end result of this initial step as the starting situation for all subsequent calculations. Set II requires no two-step procedure.

2.5. Numerical methods

We solve the model differential equations in the described model domain with a code that is based on the finite element package SEPRAN (Segal and Praagman, 2000). Equations for mass and momentum are solved simultaneously with a penalty function method with extended quadratic triangular elements, using a direct solver for resulting algebraic equations of the discretized Stokes equation. The time-dependent temperature equation is integrated with a predictor–corrector scheme on linear sub-elements of the velocity elements (van den Berg et al., 1993). For the advection of the compositional field and the determination of the basalt-to-eclogite phase change kinetics, we developed a tracer particle method. Approximately 500,000 particles are advected with a second (Predictor) or fourth (Corrector) order Runge–Kutta scheme (Press et al., 1992). Interpolation from the finite elements to the particles (to obtain the local velocity of the function field value)

is performed with a quadratic or linear interpolation inside the finite element in which the particle is positioned. Interpolation from the particles to the finite elements is performed with either a Shepard interpolation (Shepard, 1968) or a particle-in-cell interpolation (Hockney and Eastwood, 1988; Birdsall and Langdon, 1991). After particle advection, the basalt-to-eclogite phase function is updated by time integration at each particle location in a predictor–corrector technique, with an (explicit) Euler method in the predictor, and a Crank–Nicolson trapezium rule in the corrector.

3. Mechanisms for flat subduction

3.1. Observations and input parameters

In this study, we aim to examine the circumstances for which flat subduction can be expected. To gain confidence in the model results, and the choice of the set of model parameters, we compare the results of the model calculations with observations from flat slab areas on the Earth. Around the Pacific, flat subduction occurs at several locations (Gutscher et al., 2000). One of the best studied areas of flat subduction is South Peru, and we applied our numerical model to that specific area. There, the flat slab is possibly the result of a combination of the proposed mechanisms: South America moves westward with about 3 cm per year (Olbertz et al., 1997), and has the Nazca Ridge subducting at the location where the flat slab is observed. Further north or south, where no plateau is subducting, the dip angle is much steeper. The Nazca Ridge has a crustal thickness of about 18 km (McGeary et al., 1985). The convergence rate of the South American plate and the Nazca plate is 6.7 cm per year (Olbertz et al., 1997), and the age of the subducting slab is around 44 Ma.

3.2. A parameter investigation: the Peru subduction area

To quantify and better constrain the effects of the proposed flat subduction mechanisms, discussed above, we further elaborated the model results that were obtained for the Peru subduction region in (van Hunen et al., 2002a). We will briefly revisit this model, and then apply the results to better quantify the contributions of those mechanisms to other flat slab areas.

We performed model calculations for the Peru subduction zone with parameter settings as discussed above. We kept all model parameters constant, except for the upper mantle viscosity, and the basalt-to-eclogite phase change kinetics. The upper mantle viscosity is described in terms of its average effective viscosity $\bar{\eta}_{UM}$. We varied the prefactor A of Eq. (6) such that we obtained a $\bar{\eta}_{UM}$ of 2, 3.5, and 6.5×10^{20} Pa s, to approximately span the range that was suggested by observations as discussed in Section 2.2. Applied rheological parameters are given in Table 2. We varied T_{tr} between 400 and 800 °C, as suggested from geological observations (e.g. Austrheim, 1998). We fixed the yield viscosity η_y to a rather arbitrarily chosen value of $\tau_y = 300$ MPa. A mantle wedge associated with the dehydration of the subducting slab (van Hunen et al., 2002b) was imposed with a one order of magnitude lower viscosity than the rest of the mantle under similar p-T-conditions, and the lateral and depth extent of weakened part of the mantle wedge was assumed to be 250 and 40 km, respectively, measured from the mantle wedge corner. Other model parameters values are given in Table 1.

A typical model result with $\bar{\eta}_{UM} = 3.5 \times 10^{20}$ Pa s, and $T_{tr} = 700$ °C for a subducting oceanic plateau is given in Fig. 3. It shows that the subducting slab starts flattening as soon as the oceanic plateau has subducted below the overriding plate. The thicker weak crust of the plateau forms a better lubrication between the two converging plates than normal oceanic crust does, and therefore might change the subduction dynamics somewhat. However, it is primarily due to the buoyancy of that thicker crust that flat subduction sets in. For each of the relevant combinations of T_{tr} and $\bar{\eta}_{UM}$, we calculated the resulting flat slab length after 15 Ma after the model start. We defined the length of the flat slab as the horizontal shift with respect to the starting situation of the rheologically strongest part of the slab at 200 km depth. Fig. 4 gives a compilation of the model results, and shows that both an increase in the average mantle viscosity and an increased transition temperature result in a longer flat slab section. For calculations with $\bar{\eta}_{UM} = 6.5 \times 10^{20}$ Pa s, all slabs, regardless of the presence of a plateau, will go flat. Since this does not correspond to the observation that flat subduction at Peru is only observed where a plateau enters the trench, we can rule out those parameter combinations from being realistic. Similarly, all calculations

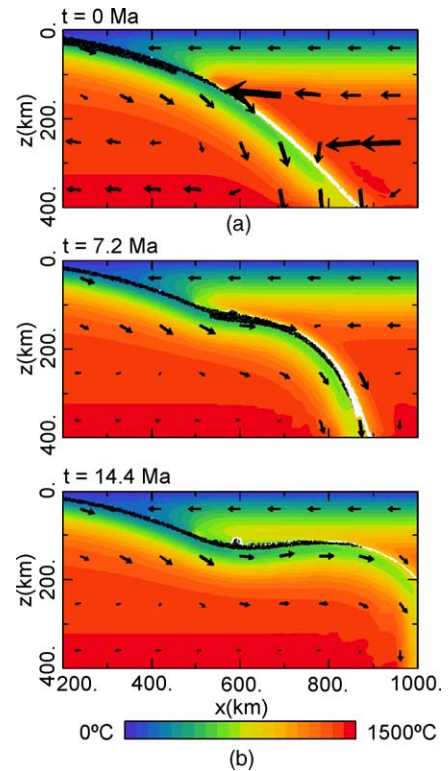


Fig. 3. Model result of a subducting oceanic plate with an oceanic plateau that enters a subduction zone below 3 cm per year trenchward moving continent. The situation displays the slab geometry at Peru. Before the oceanic plateau subduction is steep, and gradually a flat slab segment is formed due to the buoyancy of the oceanic plateau.

with $T_{tr} = 400$ or 500 °C can be discarded, because these show steep subduction, even in the presence of a plateau. We selected three parameter combinations as representative for the Peru subduction area: the $T_{tr} = 600$ and 700 °C models with $\bar{\eta}_{UM} = 3.5 \times 10^{20}$ Pa s, and the $T_{tr} = 800$ °C model with $\bar{\eta}_{UM} = 2 \times 10^{20}$ Pa s. We refer to those as models A–C, respectively. Table 3 lists the applied models in this study.

We further determined the relative importance of effects of the overriding lithosphere, and subducting plateau on the extent of the flat slab area. We did so by increasing or decreasing the crustal thickness of the plateau in each of the models A–C by 11 km, i.e. to 29 km (to which we refer to as models A⁺, B⁺, and C⁺, respectively), or 7 km (models A[−], B[−], and C[−], respectively). See Table 3 for a description of each

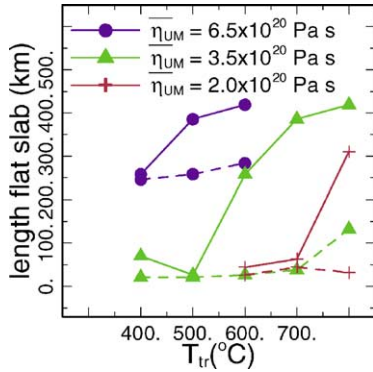


Fig. 4. Length of the flat slab segment at model time $t = 14.4$ Ma for several values of the transition temperature T_{tr} and average upper mantle viscosity $\bar{\eta}_{UM}$. Solid lines represent situations with a plateau, dashed lines without. Only the $T_{tr} = 600$ and 700 °C calculations with intermediate mantle strength, and the $T_{tr} = 800$ °C with the weakest mantle show the observed characteristics at Peru, i.e. flat subduction with a plateau, and steep without. Figure from (van Hunen et al., 2002a).

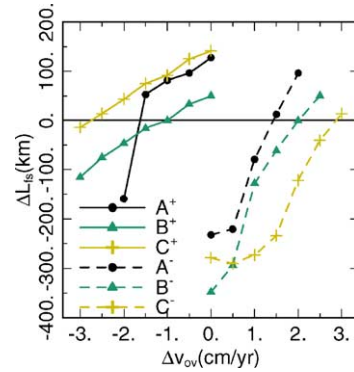


Fig. 5. Relative importance of the overriding plate motion and plateau subduction for modified versions of models A–C at model time $t = 15$ Ma. Lengths of the flat slab are for models with a ‘twice-as-thick’ plateau (solid lines) and without a plateau (dashed lines) for several overriding plate motion adjustments (with respect to the default overriding plate motion of 3 cm per year at Peru). Flat slab length differences ΔL_{fs} are measured with respect to the lengths obtained in model A–C. Figure modified after (van Hunen et al., 2002a).

model. The decrease essentially replaces the plateau by an oceanic crust with normal thickness, while the increase ‘doubles’ the plateau thickness. The underlying harzburgite thickness is proportionally adjusted. This change in plateau thickness has an influence on the flat slab length, and we tried to compensate this effect by adjusting the overriding plate motion so that we

again obtain approximately the original flat slab length from models A–C, respectively. By doing so, we have a measure to compare the effects of the plateau and the overriding lithosphere. Results for this procedure for each of the models A⁺, B⁺, C⁺, A⁻, B⁻, and C⁻ are shown in Fig. 5. The changed plateau thickness is roughly compensated by $\Delta v_{ov} \approx 1.5$ cm per year

Table 3
Model calculations

Model	Age (Ma)	T_{tr} (°C)	$\bar{\eta}_{UM}$ ($\times 10^{20}$ Pa s)	τ_y (MPa)	WMW ($\times 1000$ km ²)	v_{ov} (cm per year)	D_{cr} (km)	T_{pot} (°C)
A	45	600	3.5	300	10	3	18	1300
A ⁺	45	600	3.5	300	10	0–3	29	1300
A ⁻	45	600	3.5	300	10	3–6	7	1300
B	45	700	3.5	300	10	3	18	1300
B ⁺	45	700	3.5	300	10	0–3	29	1300
B ⁻	45	700	3.5	300	10	3–6	7	1300
C	45	800	2.0	300	10	3	18	1300
C ⁺	45	800	2.0	300	10	0–3	29	1300
C ⁻	45	800	2.0	300	10	3–6	7	1300
D45	45	400–800	2, 3.5, 6.5	200, 300, 500	6, 10, 24	1–5	7	1300
D37	36	400–800	2, 3.5, 6.5	200, 300, 500	6, 10, 24	1–5	7	1300
D25	22	400–800	2, 3.5, 6.5	200, 300, 500	6, 10, 24	1–5	7	1300
E45	45	600–800	2, 3.5, 6.5	200, 300	6, 10, 24	0	18	1300
E37	36	600–800	2, 3.5, 6.5	200, 300	6, 10, 24	0	18	1300
E25	22	600–800	2, 3.5, 6.5	200, 300	6, 10, 24	0	18	1300
E15	15	600–800	2, 3.5, 6.5	200, 300	6, 10, 24	0	18	1300
F	45	400–800	10	200	0	5	7, 9, 11	1300, 1338, 1375

(for the stronger mantle models) to 3 cm per year (for the weaker mantle model) change in the overriding plate motion. Taken the observed Nazca Ridge crustal thickness, and the South-American absolute plate motion, these model calculations suggest that the effect of the South-American plate motion is roughly once to twice as important as the effect of the subducting Nazca Ridge.

3.3. The influence of each of the mechanisms separately on the subduction dip angle

Results from the Section 3.2 show that a combination of each of the proposed mechanisms, i.e. trenchward overriding plate motion, a subducting oceanic plateau, and possibly slab suction forces, can result in shallow flat subduction. Next, we will determine the applicability of this model to other present-day flat subduction sites, where not all three mechanisms seem to be present. If we remove one of the mechanisms, the length of the flat slab segment will diminish or vanish completely. We used the Peru model to investigate how the model parameters should be changed to induce flat subduction with only the presence of an overriding continent, or a subducting oceanic plateau.

To do so, we started with Peru model A⁻ (i.e. without the oceanic plateau, see Table 3). Fig. 4 shows that this model does not show any flat subduction. We systematically changed some of the important physical model parameters separately in this model to observe its influence on the flat slab length. We refer to this model as model D (see again Table 3). The dynamics of subducting plates of three different ages at the trench was examined: 45 Ma (model D45), 36 Ma (D36), and 22 Ma (D22). We varied the average upper mantle viscosity value of 3.5×10^{20} Pa s in model D to the smaller and larger values of 2 and 6.5×10^{20} Pa s. Furthermore, we varied the overriding plate velocity $v_{ov} = 3$ cm per year with ± 2 cm per year, the maximum yield stress τ_y of the material from 300 MPa (medium yield stress model or MYS model) to 200 (small YS or SYS model) and 500 MPa (large YS or LYS model), and the transition temperature T_{tr} between 400 and 800 °C. Finally, the size of the weak part of the mantle wedge was changed from horizontal and vertical dimensions of 250 km \times 40 km (referred to as the medium weak mantle wedge (WMW) or MWMW model) to a smaller and larger weak man-

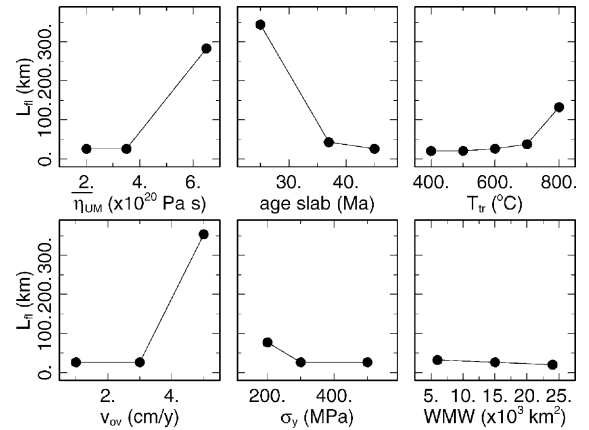


Fig. 6. Compilations of model calculations without an oceanic plateau. Several important model parameters are varied around the values from Peru model A. Most important parameters are the average upper mantle viscosity $\bar{\eta}_{UM}$, age of the slab, and overriding plate velocity v_{ov} , while eclogitisation kinetics (varied through variation in T_{tr}), slab yield stress τ_y and size of the weak mantle wedge seem to be of minor importance.

tle wedge area of 150 km \times 40 km (small WMW or SWMW), and 400 km \times 60 km (large WMW or LWMW), respectively. Results are displayed in Fig. 6. Lowering the age of the slab, increasing v_{ov} , or increasing the average mantle viscosity $\bar{\eta}_{UM}$ all result in a development of a flat slab segment. Effects of the transition temperature T_{tr} and the slab strength τ_y are less important under these circumstances. A change in the size of the weak mantle wedge does seem to have even less influence. These results suggest that the parameter combination of Peru model A is already quite close to the settings that are needed for a flat slab, because only a slight change in any of the important model parameters already leads to a flat slab.

We continue with the examination of the situation without an overriding plate motion. We adapted the Peru model B (i.e. with $\bar{\eta}_{UM} = 3.5 \times 10^{20}$ Pa s and $T_{tr} = 700$ °C) to a new model E by setting the overriding plate motion to $v_{ov} = 0$ cm per year. Not surprisingly, this immediately results in the absence of flat subduction. To obtain a smaller subduction dip angle again, we have to modify other model parameters to favor flat subduction again. One obvious choice for such modification is to reduce the age of the subducting plate: the age of the subducting plate at Peru is about 45 Ma, but at several other flat slab areas

(Nankai Trough, Mexico, Cascades) the age is much smaller (Jarrard, 1986). Other parameters to be varied are the ones that are not well constrained, such as the extent of the weak mantle wedge, and the yield stress of the material. We refer to model E with a 45 Ma old slab as model E45. We included the dynamics for models with younger slab ages of 36 Ma (model E36), 22 Ma (model E22), and 15 Ma (model E15), different sizes of the weak mantle wedge, and models with a smaller material yield stress of 200 MPa. Remarkably, we found that changing only a single parameter within these ranges doesn't change the dip angle of the subducting plate significantly, and flat subduction is not obtained in any of these situations. Only the SWMW or SYS model obtain a modest amount of flat subduction for model E22, whereas a combination of SYS and SWMW is necessary to also obtain some flat subduction for model E36. In none of the situations, flat subduction was observed for model E45.

We used model E22 and E36 to investigate again the influence of several model parameters in a systematic way. We varied one parameter at the time, while keeping the others to their default values: 3.5×10^{20} Pa s mantle stress, 200 MPa yield stress, 700 °C transition temperature, and a 50×10^3 km² weak mantle wedge per unit length of the trench. Results are shown in Fig. 7. Again, the slab age and mantle strength turn out to play an important role. Also the transition temperature T_{tr} is important, as suggested as well by the Peru model results above, while the yield stress of the slab has a more modest influence. The effect of the size of the weak mantle wedge is puzzling: although the WMW-size seems to have an influence, there is not a clear preference for a large or small WMW. Qualitatively, the parameter dependence is comparable to the results, observed in (van Hunen et al., 2002b), where a similar study was performed under somewhat different model parameter settings. The reference model from which those model parameter variations were performed was more favorable for flat subduction, and the length of the flat segment in those calculations was on average higher. The model parameters in this study are chosen with the use of observations from Peru, which gives more confidence in the choice.

The response of all models D and E (see Table 3) to most of the changes in the model parameters in this section is fairly well understood. Both a high age and a rapid basalt-to-eclogite formation will increase the av-

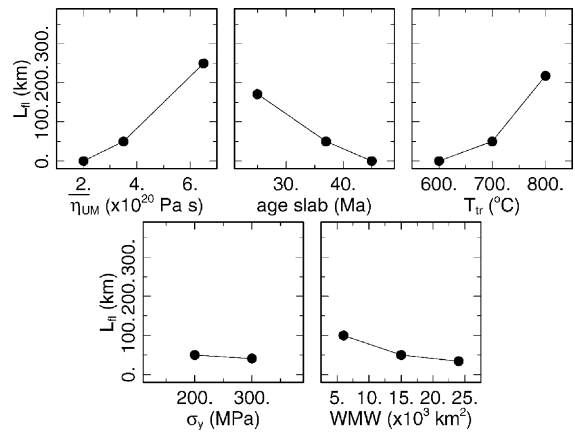


Fig. 7. Compilations of model calculations (model E) without an overriding plate motion. Important model parameters are varied for a 22 and 36-Ma old subducting slab with maximum yield stress $\tau_y = 200$ MPa. Most important parameters are the average upper mantle viscosity $\bar{\eta}_{UM}$, age of the slab, and eclogitisation kinetics. The effect of the slab yield stress τ_y is of minor importance, while the effect of the weak mantle wedge is not clear.

erage density of the subducting slab, and consequently a larger buoyancy force is necessary to flatten the slab. For the overtrusting plate model, both an increased overriding plate motion v_{ov} and an increased average upper mantle viscosity $\bar{\eta}_{UM}$ will increase the reaction force of the mantle in response to forced deformation induced by the forced subduction of the underthrust plate. This will lead to a better development of a flat slab segment. For the subducting plateau model, the positive effect of an increase in mantle viscosity on the length of the flat slab is less clear. The most likely explanation for this influence is that an overall increase of the mantle strength also makes the mantle wedge stronger. This can have two effects that counteract each other: (1) It requires larger forces to adapt the shape of the mantle wedge when the dip angle decreases in the creation of a flat slab (van Hunen et al., 2002b), and (2) It increases the plate suction forces that tend to enhance flat subduction (Stevenson and Turner, 1977; Tovish et al., 1978). The $\bar{\eta}_{UM}$ -variation plot in Fig. 7 suggests that the second effect dominates the first one. The effect of the size of the weak mantle wedge is complicated for the same reasons. This study clearly shows that the size and weakness of the mantle wedge are important in the development of flat subduction, which is a direct indication for the significance of the

slab suction forces. Therefore, more detailed studies to the effect of size and strength of the weakened mantle wedge, such as done by [Billen and Gurnis \(2001\)](#), should be applied to the flat subduction models to fully understand its influence, possibly including a dynamically more self-consistent way of rheological weakening in the mantle wedge by incorporating devolatilizing subducting slabs and resulting mantle wedge hydration ([Iwamori, 1998](#)).

In general, we observed that flat subduction occurs more easily due to only an overthrusting continent than due to a subducting plateau alone for the examined range of model parameters. Our results show that the proposed large flat slab region below North-America during the Laramide orogeny (e.g. [Dickinson and Snyder, 1978](#); [Bird, 1988, 1998](#)) was very likely and even almost inevitable if the 5 cm per year North-American plate motion in a hotspot reference frame ([Engelbreton et al., 1985](#)) is correctly interpreted as the overriding plate motion. Several of the present-day flat slab regions, however, are not correlated to overthrusting continents. This study shows that favorable conditions for flat subduction due to the single effect of a subducting oceanic plateau are less common. Adding the fact that the two-dimensional model probably overestimates the effect of a subducting plateau on the dip angle ([van Hunen et al., 2002b](#)), we are somewhat puzzled about the observed, rather striking correlation between subducting plateaus and the location of flat subduction ([Gutscher et al., 2000](#)). However, we are aware of the fact that the plateau model contains several poorly constrained model parameters. The two most important of those are probably the strength of the subducting slab, and the extent of the basalt metastability after subduction, in which the effects of hydration and deformation are probably important, but highly unconstrained ([Rubie, 1990](#)). Better constraints on those parameters may provide narrower constraints on the plateau effect on the subduction dynamics.

4. Flat subduction in a younger, hotter Earth

We extended this parameter study by examining the influence of the mantle temperature on the viability of flat subduction, using model F (see [Table 3](#)). We gradually increased the potential mantle temper-

ature from a present-day value, which was taken to be 1300 °C, to simulate the situation of a younger Earth. This mantle temperature increase will have two important effects on the subduction dynamics: (1) It will lead to a thicker crust and harzburgite layer, and therefore to more compositional buoyancy of the oceanic plate. Here, we used the crustal and harzburgitic layer thicknesses from ([Vlaar and van den Berg,, 1991](#)). (2) It will decrease the temperature-dependent mantle viscosity, which will lead to a more vigorous convective mantle regime. Since we calibrate both the thickness of the crust and the mantle viscosity to present-day observations, the actual choice of the potential temperature T_{pot} for the present-day situation is not important, and only the increase with respect to that value for a younger Earth is relevant. Since for a hotter mantle not just patches of the oceanic crust are thickened, but the whole plate has a thicker crust, we cannot apply the assumption that the average plate remains negatively buoyant, and will drive the subduction. Therefore, to obtain subduction even in the case of buoyant oceanic lithosphere with a thick crust, we again imposed an (arbitrarily chosen) overthrusting plate velocity of 5 cm per year. Furthermore, the subducting plate has a relatively young age of 45 Ma, consistent with the idea that old oceanic lithosphere cannot account for a large heat flow that has cooled the Earth in the past ([Davies, 1992](#)). We chose the maximum yield stress $\tau_y = 200$ MPa, used a relatively strong average mantle viscosity of about 10^{21} Pa s, and ignored possible effects of a weak mantle wedge. Applied rheological parameters are given in [Table 2](#). [Fig. 8](#) shows the resulting slab dynamics for several mantle temperatures. For this calculation, we used a modest basalt metastability by choosing $T_{\text{tr}} = 500$ °C. The model simulation with $T_{\text{pot}} = 1300$ °C displays the present-day situation, and results are comparable to overriding plate velocity results in the former section. A small mantle temperature increase of 38 K basically shows no difference in the slab behavior. But for a similar mantle temperature rise to $T_{\text{pot}} = 1375$ °C the subduction style is steep. This variation in subduction style is reflected in the convergence velocity between the overriding and the subducting plate: during flat subduction, the subducted lithosphere is positioned rather passively below the overthrusting lithosphere, in which the convergence velocity is approximately the imposed overriding plate motion.

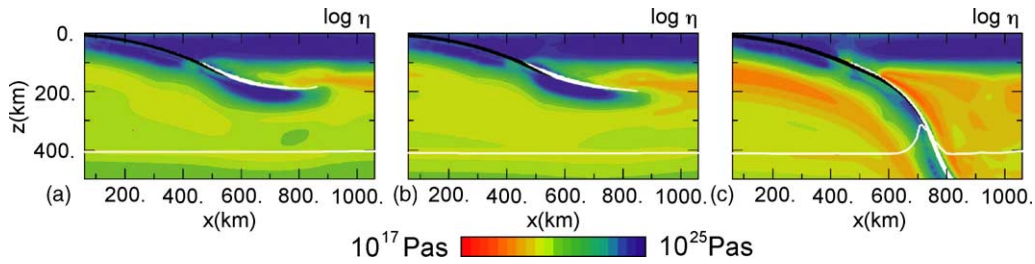


Fig. 8. Viscosity plot of subduction process below an trenchward moving overriding continent at $t = 12.8$ Ma after model initiation. Colors represent the effective mantle viscosity, while black and white areas refer to basaltic and eclogitic crust, respectively. Potential temperature: (a) $T_{\text{pot}} = 1300^\circ\text{C}$, (b) $T_{\text{pot}} = 1338^\circ\text{C}$, and (c) $T_{\text{pot}} = 1375^\circ\text{C}$. The white line at 400 km depth represents the mantle phase transition at that depth.

But if steep subduction occurs, the slab hangs in the mantle, and its weight can be effectively transmitted to the oceanic plate at the surface. This causes slab pull to act as an additional force to the subduction system, which rapidly increases the convergence rate. This allows for a more compressed representation of the subduction dynamics in Fig. 9. This plot shows the resulting convergence rate for different mantle temperatures and different eclogite-formation rates, parameterized through the transition temperature T_{tr} . For $T_{\text{pot}} = 1300$ and 1338°C , the convergence rates differ little for different transition temperatures: for high T_{tr} , convergence is a little slower than for low T_{tr} , which reflects the resistance of the buoyant, metastable basaltic crust to subduction. Only for $T_{\text{pot}} = 1375^\circ\text{C}$, convergence rates depend largely on the the transition temperature. For low T_{tr} , eclogite forms quickly during subduction, which leads to steep subduction, effective transmission of slab pull to the oceanic plate at the surface, and therefore to an

increased convergence rate. Only for $T_{\text{tr}} = 800^\circ\text{C}$, the convergence rate remains low, and indeed for this calculation flat subduction is still observed. The convergence rate, however, is significantly lower than the overriding plate motion of 5 cm per year. This represents a dynamical state that may be best described by a mix of pure collision (in which case the convergence rate decreases to zero), and passive subduction (in which case the convergence rate equals the overriding plate motion). Fig. 8c further shows the localized low viscosity region surrounding the cold slab. The effect of high slab velocity (and resulting high strain rate) in combination with composite rheology illustrates the lubricating effect of strain rate localization (van den Berg and Yuen, 1997). Model calculations were also performed at even larger than $T_{\text{pot}} = 1375^\circ\text{C}$ mantle temperatures. All these calculations showed steep subduction for $T_{\text{tr}} \leq 600^\circ\text{C}$, and no subduction at all, or rather collision, for $T_{\text{tr}} = 800^\circ\text{C}$. In general, we can conclude from these results that flat subduction in a

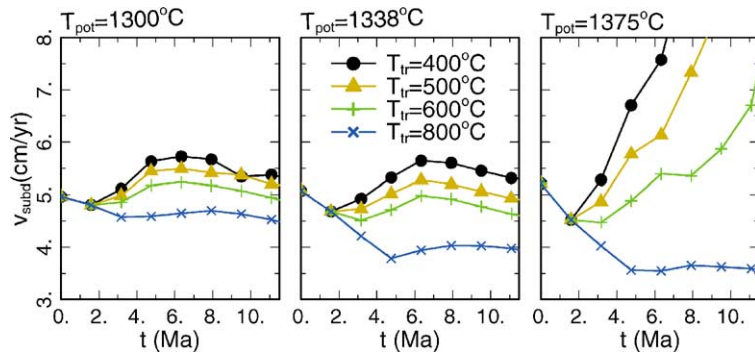


Fig. 9. Convergence velocity during subduction below a trenchward moving overriding continent for different values of the potential temperature T_{pot} and transition temperature T_{tr} .

much hotter Earth is not viable. This result contradicts earlier theories that flat subduction was more abundant in a hotter Earth as a result of the buoyant character of the subducting plates (Vlaar, 1986; Abbott et al., 1994). The presented results put important constraints on the geodynamical regime in a hotter Earth, as discussed by, e.g. Hamilton (1998), de Wit (1998).

5. Conclusions

Several mechanisms have been proposed to explain the worldwide occurrence of flat subduction at approximately 10% of the trenches. We grouped these mechanisms into three categories: (1) subduction of lithosphere with increased buoyancy because of its young age or the presence of an oceanic plateau; (2) subduction below an trenchward moving overthrusting continent; and (3) slab suction forces in the mantle wedge. We investigated the effects of each of these mechanisms through numerical modeling experiments. Comparison of model results of the subduction geometry near Peru with the observed geometry allows for calibration of several of the model parameters, from which we conclude that the average mantle viscosity ranges between 2 and 3.5×10^{20} Pa s, and basalt should be able to survive temperatures of 600 to 800 °C. We used this model to quantify the circumstances for which we expect shallow flat subduction if an overriding continent or an oceanic plateau is absent. We conclude that an overriding continent easily provides the circumstances for flat subduction. A slightly higher overriding plate motion, average mantle viscosity, as well as a slightly weaker or younger slab than is observed near Peru already results in flat subduction. An oceanic plateau without an overriding plate motion seems to be much less capable of developing low-to-zero angle subduction, and only a combination of the changes, mentioned above, gives rise to flat subduction. The plate suction forces play an important role, but further research will be needed to quantify the effects of the mantle wedge viscosity and the hydrous weakening of the mantle wedge due to the devolatilisation of the subducting slab. We also applied the numerical situation to a hotter mantle to simulate the dynamics of a younger Earth. We used this model to determine the viability of flat subduction in this situation. The resulting increase in the oceanic plate buoy-

ancy and the weakening of the mantle counteract each other, but the rheological effect seems to dominate, because flat subduction is not observed for even a modest mantle temperature increase of 75 K. This rules out the previously suggested scenario that flat subduction was a more wide-spread phenomenon in the past.

Acknowledgements

We would like to thank Masanori Kameyama for a thorough and constructive review, which helped to improve the manuscript substantially. This work was sponsored by the Stichting Nationale Computerfaciliteiten (National Computing Facilities Foundation, NCF) for the use of supercomputer facilities, with financial support from the Nederlandse Organisatie voor Wetenschappelijk Onderzoek (Netherlands Organization for Scientific Research, NWO).

References

- Abbott, D., Drury, R., Smith, W.H.F., 1994. Flat to steep transition in subduction style. *Geology* 22, 937–940.
- Ahrens, T.J., Schubert, G., 1975. Gabbro-eclogite reaction rate and its geophysical significance. *Rev. Geophys. Space Phys.* 13 (2), 383–400.
- Austrheim, H., 1998. Influence of fluid and deformation on metamorphism of the deep crust and consequences for the geodynamics of collision zones. In: Hacker, B., Liou, J. (Eds.), *When Continents Collide: Geodynamics and Geochemistry of Ultrahigh-Pressure Rocks*. Kluwer Academic Publishers, pp. 297–323.
- Bickle, M.J., 1986. Implications of melting for stabilisation of the lithosphere and heat loss in the Archaean. *Earth Planet. Sci. Lett.* 80, 314–324.
- Billen, M.I., Gurnis, M., 2001. A low viscosity wedge in subduction zones. *Earth Planet. Sci. Lett.* 193, 227–236.
- Bird, P., 1988. Formation of the rocky mountains, Western United States: a continuum computer model. *Science* 239, 1501–1507.
- Bird, P., 1998. Kinematic history of the Laramide orogeny in latitudes 35–49° N, western United States. *Tectonics* 17 (5), 780–801.
- Birdsall, C.K., Langdon, A.B., 1991. *Plasma Physics via Computer Simulation*. McGraw-Hill Inc.
- Bos, B., Spiers, C.J., 2002. Frictional-viscous flow of phyllosilicate-bearing fault rock: microphysical model and implications for crustal strength. *J. Geophys. Res.* 107 (B2), 10.1029/2001JB000301.
- Cristan, Y., 1982. The transition from high-temperature creep to fracture in Maryland diabase. *J. Geophys. Res.* 87, 6781–6790.

- Chapman, D.S., 1986. Thermal gradients in the continental crust. In: Dawson, J.B., Carswell, D.A., Hall, J., Wedepohl, K.H. (Eds.), *The Nature of the Lower Continental Crust*. Geological Society, pp. 63–70.
- Cížková, H., van Hunen, J., van den Berg, A.P., Vlaar, N.J., 2002. The influence of rheological weakening and yield stress on the interaction of slabs with the 670 km discontinuity. *Earth Planet. Sci. Lett.* 199, 447–457.
- Cross, T.A., Pilger Jr., R.H., 1978. Tectonic controls of late Cretaceous sedimentation, western interior, USA. *Nature* 274, 653–657.
- Davies, G.F., 1992. On the emergence of plate tectonics. *Geology* 20, 963–966.
- de Wit, M.J., 1998. On Archean granites, greenstones, cratons and tectonics: does the evidence demand a verdict? *Precambrian Res.* 91, 181–226.
- Dickinson, W., Snyder, W., 1978. Plate tectonics of the Laramide orogeny. *Geol. Soc. Am. Mem.* 151, 355–366.
- Engelbreton, D.C., Cox, A., Gordon, R.G., 1985. Relative motions between oceanic and continental plates in the Pacific basin. *Geol. Soc. Am.* 286, 1–59 (special paper).
- England, P., Bickle, M., 1984. Continental thermal and tectonic regimes during the Archaean. *J. Geol.* 92, 353–367.
- Giunchi, C., Ricard, Y., 1999. High-pressure/low-temperature metamorphism and the dynamics of an accretionary wedge. *Geophys. J. Int.* 136, 620–628.
- Gutscher, M.-A., Spakman, W., Bijwaard, H., Engdahl, E., 2000. Geodynamics of flat subduction: Seismicity and tomographic constraints from the Andean margin. *Tectonics* 19 (5), 814–833.
- Hacker, B.R., 1996. Eclogite formation and the rheology, buoyancy, seismicity and H₂O content of oceanic crust. In: *Subduction: Top to Bottom*. AGU Monogr, pp. 337–346.
- Hamilton, W.B., 1998. Archean magmatism and deformation were not products of plate tectonics. *Precambrian Res.* 91, 143–179.
- Herzberg, C., 1992. Depth and degree of melting of komatiites. *J. Geophys. Res.* 97, 4521–4540.
- Hockney, R.W., Eastwood, J.W., 1988. *Computer Simulations Using Particles*. IOP Publishing Ltd., Bristol.
- Iwamori, I., 1998. Transportation of H₂O and melting in subduction zones. *Earth Planet. Sci. Lett.* 160, 65–80.
- Jarrard, R.D., 1986. Relations among subduction parameters. *Rev. Geophys.* 24 (2), 217–284.
- Ji, S., Zhao, P., 1994. Layered rheological structure of subducting oceanic lithosphere. *Earth Planet. Sci. Lett.* 124, 75–94.
- Kameyama, M., Yuen, D.A., Karato, S.-I., 1999. Thermal-mechanical effects of low-temperature plasticity (the Peierls mechanism) on the deformation of a viscoelastic shear zone. *Earth Planet. Sci. Lett.* 168, 159–172.
- Karato, S.-I., Riedel, M.R., Yuen, D.A., 2001. Rheological structure and deformation of subducted slabs in the mantle transition zone: implications for mantle circulations and deep earthquakes. *Phys. Earth Planet. Int.* 127, 83–108.
- Karato, S.-I., Wu, P., 1993. Rheology of the upper mantle: a synthesis. *Science* 260, 771–778.
- Kohlstedt, D.L., Evans, B., Mackwell, S.J., 1995. Strength of the lithosphere: constraints imposed by laboratory experiments. *J. Geophys. Res.* 100 (B9), 17587–17602.
- Lambeck, K., Johnston, P., 1998. The viscosity of the mantle: Evidence from analysis of glacial-rebound phenomena. In: Jackson, I. (Ed.), *The Earth's Mantle: Composition, Structure and Evolution*. Cambridge University Press, pp. 461–502.
- Lambeck, K., Smither, C., Johnston, P., 1998. Sea-level change, glacial rebound and mantle viscosity for northern Europe. *Geophys. J. Int.* 134, 102–144.
- Mackwell, S.J., Zimmerman, M.E., Kohlstedt, D.L., 1998. High-temperature deformation of dry diabase with application to tectonics on Venus. *J. Geophys. Res.* 103 (B1), 975–984.
- McGeary, S., Nur, A., Ben-Avraham, Z., 1985. Spatial gaps in arc volcanism: the effect of collision or subduction of oceanic plateaus. *Tectonophysics* 119, 195–221.
- Olbertz, D., Wortel, M.J.R., Hansen, U., 1997. Trench migration and subduction zone geometry. *Geophys. Res. Lett.* 24, 221–224.
- Press, W.H., Teukolsky, S.A., Vetterling, W.T., Flannery, B.P., 1992. *Numerical Recipes in Fortran, The Art of Scientific Computing*. Cambridge University Press.
- Riedel, M.R., Karato, S.-I., 1996. Microstructural development during nucleation and growth. *Geophys. J. Int.* 125, 397–414.
- Rubie, D., 1990. Role of kinetics in the formation and preservation of eclogites. In: Carswell, D.A. (Ed.), *Eclogite Facies Rocks*. Blackie, Glasgow, pp. 111–140.
- Sacks, I.S., 1983. The subduction of young lithosphere. *J. Geophys. Res.* 88 (B4), 3355–3366.
- Saunders, A., Tarney, J., Kerr, A., Kent, R., 1996. The formation and fate of large oceanic igneous provinces. *Lithos* 37, 81–95.
- Schmelting, H., Monz, R., Rubie, D.C., 1999. The influence of olivine metastability on the dynamics of subduction. *Earth Planet. Sci. Lett.* 165, 55–66.
- Segal, A., Praagman, N.P., 2000. The sepran package. Technical report, <http://dutita0.twi.tudelft.nl/sepran/sepran.html>.
- Shelton, G., Tullis, J., 1981. Experimental flow laws for crustal rocks. *Eos. Trans. Am. Geophys. Union* 62 (17), 396.
- Shepard, D., 1968. A two-dimensional interpolation function for irregularly-spaced data. In: *Proceedings of the 23rd National Conference*. ACM, New York, pp. 517–524.
- Spencer, J.E., 1996. Uplift of the Colorado Plateau due to lithosphere attenuation during Laramide low-angle subduction. *J. Geophys. Res.* 101 (B6), 13595–13609.
- Stevenson, D.J., Turner, S.J., 1977. Angle of subduction. *Nature* 270, 334–336.
- Stöckhert, B., Renner, J., 1998. Rheology of crustal rocks at ultrahigh pressure. In: Hacker, B., Liou, J. (Eds.), *When Continents Collide: Geodynamics and Geochemistry of Ultrahigh-Pressure Rocks*. Kluwer Academic Publishers, pp. 57–95.
- Tovish, A., Schubert, G., Luyendyk, B.P., 1978. Mantle flow pressure and the angle of subduction: non-Newtonian corner flows. *J. Geophys. Res.* 83 (B12), 5892–5898.
- van den Berg, A.P., van Keken, P.E., Yuen, D.A., 1993. The effects of a composite non-Newtonian and Newtonian rheology on mantle convection. *Geophys. J. Int.* 115, 62–78.
- van den Berg, A.P., Yuen, D.A., 1997. The role of shear heating in lubricating mantle flow. *Earth Planet. Sci. Lett.* 151, 33–42.

- van Hunen, J., van den Berg, A.P., Vlaar, N.J., 2000. A thermo-mechanical model of horizontal subduction below an overriding plate. *Earth Planet. Sci. Lett.* 182, 157–169.
- van Hunen, J., van den Berg, A.P., Vlaar, N.J., 2001. Latent heat effects of the major mantle phase transitions on low-angle subduction. *Earth Planet. Sci. Lett.* 190, 125–135.
- van Hunen, J., van den Berg, A.P., Vlaar, N.J., 2002a. The impact of the South-American plate motion and the Nazca Ridge subduction on the flat subduction below South Peru. *Geophys. Res. Lett.* 29 (14), 10.1029/2001GL014004.
- van Hunen, J., van den Berg, A.P., Vlaar, N.J., 2002b. On the role of subducting oceanic plateaus in the development of shallow flat subduction. *Tectonophysics* 352, 317–333.
- Vermeersen, L.L.A., Sabadini, R., Devoti, R., Luceri, V., Rutigliani, P., Sciarreta, C.G.B., 1998. Mantle viscosity inferences from joint inversions of Pleistocene deglaciation-induced changes in geopotential with a new SLR analysis and polar wander. *Geophys. Res. Lett.* 25 (23), 4261–4264.
- Vlaar, N.J., 1983. Thermal anomalies and magmatism due to lithospheric doubling and shifting. *Earth Planet. Sci. Lett.* 65, 322.
- Vlaar, N.J., 1986. Archaean global dynamics. *Geologie en Mijnbouw* 65, 91–101.
- Vlaar, N.J., van den Berg, A.P., 1991. Continental evolution and archaeo-sea-levels. In: Sabadini, R., Lambeck, K., Boschi, E. (Eds.), *Glacial Isostasy, Sea-Level and Mantle Rheology*. Kluwer Academic Publishers.
- Vlaar, N.J., Wortel, M.J.R., 1976. Lithospheric aging, instability and subduction. *Tectonophysics* 32, 331.
- Wortel, M.J.R., Remkes, M.J.N., Govers, R., Cloetingh, S.A.P.L., Meijer, P.T., 1991. Dynamics of the lithosphere and the intra-plate stress field. *Philos. Trans. R. Soc. Lond.* 337, 111–126.